Resonant two- or three-photon ionization of noble-gas atoms captured by time-resolved photoelectron momentum spectroscopy

Mitsuko Murakami and G. P. Zhang

Phys. Rev. A **96**, 063403 — Published 1 December 2017

DOI: 10.1103/PhysRevA.96.063403

Resonant two- or three-photon ionization of noble-gas atoms captured by time-resolved photoelectron momentum spectroscopy

Mitsuko Murakami* and G. P. Zhang

Department of Physics, Indiana State University, Terre Haute, IN 47809, USA

Abstract

We present an all-electron, ab initio calculation of time-resolved photoelectron momentum distributions (PMDs) induced by resonant two-color, two- or three-photon ionization of helium and neon atoms, as recently measured by Villeneuve *et al.* [Science **356**, 1150-1153 (2017)] using a femtosecond infrared (IR) laser pulse and an attosecond pulse train (APT) produced with high harmonic generation as an extreme ultraviolet (XUV) photon source. In contrast to a monochromatic XUV pulse commonly used at the free-electron laser facilities, an APT is broadband and ultrashort (< 1 fs), so that it could induce non-resonant one-photon transitions above ionization threshold as well as a resonantly excited state. They may interfere with each other upon subsequent absorption or emission of an IR photon, so that the resultant PMD loses clear orbital symmetry. Our time-dependent density functional calculation demonstrates that the selection of a particular excited state in the time-resolved PMD is nevertheless possible if energy and timing of an APT are adjusted properly.

* Mitsuko.Murakami@indstate.edu

I. INTRODUCTION

Resonant two-photon ionization (R2PI) occurs via absorption of two photons (generally in different colours), one tunable to scan across bound-state energy of each electron in an atom, and the other ionizing the electron from a resonantly-excited state to free partial waves. The advent of intense XUV light sources such as free electron lasers (FEL) and high harmonic generation (HHG) opened up an opportunity to study this process. Although both single-photon and multi-photon ionization of noble-gas atoms, induced by synchrotron radiation [1] and long-wavelength ($\sim$ 800 nm) femtosecond laser pulses [2], respectively, have already been studied extensively for more than a few decades, R2PI provides a superior control over the selection of a particular excited-state electron to ionize. The orbital symmetry of an ionized electron is directly reflected in the photoelectron momentum distribution (PMD) [3].

The PMD of a neon (Ne) atom following the absorption of two monochromatic XUV photons was first measured by using a 44-eV, 30-fs pulse of the free-electron laser at Hamburg (FLASH) in 2007 [4]. Their objective was to study the mechanism of double ionization, that is, in what driving-laser conditions electrons leave a parent atom sequentially through an intermediate ionic state, or directly in a correlated manner through a virtual state [5–7]; for details, see Ref. [8] and references therein. A similar measurement of a helium (He) atom in 2013 at the SPring-8 (super photon ring at 8 GeV) Compact SASE (self-amplified spontaneous-emission) Source in Ref. [9] using a monochromatic XUV pulse of energy 20-25 eV and duration $\sim$ 30 fs confirmed the even symmetry of S and D partial waves in the PMDs of a singly-ionized He via R2PI through an intermediate excited p-state, as previously predicted based on the time-dependent close-coupling method [10].

When an XUV pulse is superposed with an infrared (IR) "dressing" laser field, sidebands corresponding to absorption and emission of IR photons are produced around XUV peaks in the PMD [11]. Such PMD sidebands of a Ne atom induced by two-color (XUV+IR) photoionization were investigated at FLASH in Refs. [12, 13] using a pair of XUV ($\sim$1000 eV) and IR (800 nm) photons. The duration of an XUV pulse was short ($2-5$ fs) in Ref. [12] and long (80 fs) in Ref. [13], respectively, but the PMD sidebands in both cases exhibit strong modulations along emission angles. The observed angular variations in the PMD were interpreted as interferences between many outgoing partial waves, each with its own orbital angular momentum (S, P, D,...), intensity, and phase.

In parallel with these developments in the photoelectron momentum spectroscopy using FEL, progress in HHG to produce an attosecond pulse train (APT) of central energy $20 - 35$ eV has reached the intensity levels needed for studying R2PI in recent years [14]. A typical duration of XUV pulses in an APT is a few-hundred attoseconds, as a result of broadband high harmonic radiation, which makes it possible to resolve the electron motion in photoelectron momentum spectroscopy [15]. In 2010, sidebands in the time-resolved PMD of a He atom were produced with a dressing IR field and a delayed APT (made of seven high-harmonic fields generated from argon gas) and used to determine an atomic dipole phase which an electron acquires during R2PI [16, 17]. Their measurement, however, was not resolved in terms of emission angles. On the other hand, an angle-resolved measurement of He-atom PMDs was reported in 2011 in Ref. [18] using an IR laser pulse and its high harmonic produced via HHG. By selecting a particular harmonic, they produced a monochromatic XUV pulse of longer duration (~ 100 fs) and used it to measure the branching ratio of S and D partial waves in the PMD at different IR-laser intensities. We need to be aware that the monochromacity of an XUV pulse is compromised when synthesizing an ultrashort (< 1 fs) APT from HHG for a time-resolved measurement. The broad bandwidth of an APT implies that an electron tends to be excited into multiple energy levels (separated by the fundamental frequency of HHG) above ionization threshold via non-resonant one-photon transitions, rather than into a particular resonantly-excited state. What one expects to ionize by a combination of a dressing IR field and an APT is a wave-packet, consisting of multiple excited states of an atom. They could interfere and break the orbital symmetry in a PMD. Nevertheless, the selection of a particular excited state in R2PI is still possible in the time-resolved PMD, as we will demonstrate in this paper. Measurements using an APT as a probe are time-resolved by default. Separation of pulses in an APT produced from HHG is either half-optical cycle of a dressing IR laser field, or a full-optical cycle when the second harmonic is added to the dressing IR laser field. They can act as an extremely accurate clock in ultrafast electron dynamics, in a similar manner to how a frequency comb is used as a ruler in precision spectroscopy. Time-resolved PMD measured with an APT could offer new insights into R2PI which are otherwise not detectable with a monochromatic XUV pulse, e.g., the effects of "quantum beats" due to hyperfine levels [19].

In this paper, we calculate the time-resolved PMD of He and Ne atoms during resonant two-color, two- or three-photon ionization driven by a 20-cycle IR laser pulse and an APT,

based on the numerical solution of the time-dependent Kohn-Sham equations [20]. The energy of an XUV photon is restricted to ~ 20 eV, for which doubly excited states of He or Ne atoms are not accessible through two-photon absorption. Our results are compared with the recent PMD measurement of He and Ne atoms by Villeneuve *et al.* [21] using either a monochromatic IR laser field of frequency ω_o or a two-color IR field of frequencies ω_o and $2\omega_o$ as a dressing field, and an APT produced with their high harmonics as a resonant-excitation driver. The calculation of cross-sectional PMDs provided in their paper was based on the time-dependent Schrödinger equation in the limit of single-active-electron approximation with an effective potential of argon; they mentioned a need for calculations based on a benchmark Neon potential, and we intend to present one. We will show that the 6-lobe structure in the Ne-atom PMD (reflecting a F partial wave in the configuration space) observed by Villeneuve *et al.* can in fact also be produced with a He atom if the IR driving-laser frequency and intensity are so chosen as to induce resonant three-photon ionization (R3PI). To this end, an XUV photon contained in an APT must resonantly excite an electron in the He ground state into the $1s2p\,^1P$ excited state. The ionization of the He $2p$ excited state takes two IR photons through an intermediate $1s3d\,^1D$ excited state whose energy is roughly 1.5 eV above the $2p$ level, in resonance with the frequency of an 820-nm laser field. Alternatively, it is also possible to resonantly excite a ground-state electron in a He atom into the $1s3p\,^1P$ state with an XUV photon and subsequently ionize it with one IR photon, i.e., induce R2PI, using a 790-nm laser field. The resulting PMD will have a 4-lobe structure associated with a D partial wave. In order to observe clear orbital symmetry in the time-resolved PMD, however, the separation of XUV pulses in an APT needs to be a half-optical cycle rather than a full-optical cycle to avoid interferences between resonant and non-resonant transitions. The similar scheme works with a Ne atom, but there is an additional interference between valence electrons in the degenerate $2p$-orbital, which breaks symmetry in the Ne-atom PMD with respect to the plane perpendicular to a driving-laser polarization axis.

The paper is organized as follows. In Section II, we describe the numerical methods in our calculations based on the time-dependent density functional theory. Results are presented in Section III. The time-resolved PMDs of a He atom through R2PI or R3PI using a 20-cycle IR laser pulse and an APT, whose central frequency is set around the 15th harmonic of the IR pulse, are presented first in Sec. III A. We demonstrate that the PMD has even (S, D,

...) symmetry when the driving-laser frequency and intensity are adjusted for two-photon (XUV+IR) resonant transition through an intermediate excited state of $1s3p\,^1P$, or odd (P, F, ...) symmetry when they are adjusted for three-photon (XUV+IR+IR) ionization through $1s2p\,^1P$ and $1s3d\,^1D$. We discuss two different strategies for a time-resolved measurement, one where each XUV pulse in an APT is separated by a half-optical cycle and the other by a full-optical cycle. Only the former type of an APT can isolate a resonantly excited state in the PMD, free of interferences with non-resonantly excited ones. The PMDs of a Ne atom is presented next in Sec. III B. In addition to the orbital symmetry in the Ne-atom PMD, we investigate contributions from different orbitals of a Ne atom in the amount of total electron yield in a PMD, most importantly those from the degenerate $2p$-orbital. Section IV summarizes the results. Atomic units ($e = m_e = \hbar = 1$) are used throughout, unless specified otherwise.

II. METHODS

A. Time-dependent density functional theory

We solve the time-dependent Kohn-Sham equations for all electrons in an atom, given by

$$i\frac{\partial}{\partial t}\psi_{i\sigma}(\mathbf{r},t) = \mathcal{H}(\mathbf{r},t)\psi_{i\sigma}(\mathbf{r},t), \tag{1}$$

where $i = 1, 2, ..., N_\sigma$ ranges over occupied atomic orbitals, and $\sigma \in \{\uparrow, \downarrow\}$ specifies the electron spin, $\pm\frac{1}{2}$, with

$$\mathcal{H}(\mathbf{r},t) = \frac{-1}{2}\nabla^2 - \frac{Z}{r} + v_\sigma^{\mathrm{KS}}[n_\uparrow, n_\downarrow](\mathbf{r},t) + \mathbf{r}\cdot\mathbf{E}(t). \tag{2}$$

The charge number of a nucleus is equal to the total number of electrons, i.e., $Z = N_\uparrow + N_\downarrow$. The KS potential $v_\sigma^{\mathrm{KS}}[n_\uparrow, n_\downarrow](\mathbf{r},t)$ is a functional of the spin electron density

$$n_\sigma(\mathbf{r},t) = \sum_{i=1}^{N_\sigma} n_{i\sigma}(\mathbf{r},t) = \sum_{i=1}^{N_\sigma} |\psi_{i\sigma}(\mathbf{r},t)|^2. \tag{3}$$

In general, the KS potential consists of two parts, such that

$$v_\sigma^{\mathrm{KS}}[n_\uparrow, n_\downarrow](\mathbf{r},t) = V_{\mathrm{H}}[n](\mathbf{r},t) + v_\sigma^{\mathrm{xc}}[n_\uparrow, n_\downarrow](\mathbf{r},t). \tag{4}$$

The first term is the Hartree potential

$$V_{\mathrm{H}}[n](\mathbf{r},t) = \iiint \frac{n(\mathbf{r}',t)}{|\mathbf{r}-\mathbf{r}'|} d^3\mathbf{r}', \tag{5}$$

which is a functional of total electron density: $n(\mathbf{r},t) = \sum_\sigma n_\sigma(\mathbf{r},t)$. The second term in (4) is an exchange-correlation potential and needs to be approximated in practice. We employ the local density approximation (LDA) with a self interaction correction (SIC), given by [22, 23]

$$v_\sigma^{\rm xc}[n_\uparrow, n_\downarrow](\mathbf{r},t) \simeq V_\sigma^{\rm LDA}[n_\sigma](\mathbf{r},t) - V_\sigma^{\rm SIC}(\mathbf{r},t), \tag{6}$$

where

$$V_\sigma^{\rm LDA}[n_\sigma](\mathbf{r},t) = -\left(\frac{6}{\pi} n_\sigma(\mathbf{r},t)\right)^{1/3}, \tag{7}$$

and

$$V_\sigma^{\rm SIC}(\mathbf{r},t) = V_\sigma^{\rm SI}(\mathbf{r},t) + \frac{1}{n_\sigma(\mathbf{r},t)} \sum_{i=1}^{N_\sigma}{}' n_{i\sigma}(\mathbf{r},t) v_{i\sigma}(t), \tag{8}$$

with

$$V_\sigma^{\rm SI}(\mathbf{r},t) = \frac{1}{n_\sigma(\mathbf{r},t)} \sum_{i=1}^{N_\sigma} n_{i\sigma}(\mathbf{r},t) w_{i\sigma}(\mathbf{r},t), \tag{9}$$

where

$$w_{i\sigma}(\mathbf{r},t) = V_{\rm H}[n_{i\sigma}](\mathbf{r},t) - V_\sigma^{\rm LDA}[n_{i\sigma}](\mathbf{r},t). \tag{10}$$

Moreover, $v_{i\sigma}(t) \equiv \langle V_{i\sigma}^{\rm SIC}(t)\rangle - \langle w_{i\sigma}(t)\rangle$, where

$$\langle V_{i\sigma}^{\rm SIC}(t)\rangle = \iiint V_\sigma^{\rm SIC}(\mathbf{r},t) n_{i\sigma}(\mathbf{r},t)\, d^3\mathbf{r}, \tag{11}$$

and

$$\langle w_{i\sigma}(t)\rangle = \iiint w_{i\sigma}(\mathbf{r},t) n_{i\sigma}(\mathbf{r},t)\, d^3\mathbf{r}. \tag{12}$$

The asymptotic condition: $V_\sigma^{\rm SIC} \to 0$ as $r \to \infty$ requires that $v_{i\sigma} = 0$ for the highest occupied AOs (HOAOs), and thus $\sum'$ in Eq. (8) denotes the summation over all orbitals except for HOAOs [24]. We can calculate $v_{i\sigma}(t)$ non-iteratively as [25]

$$v_{i\sigma}(t) = \sum_{j=1}^{N_\sigma}{}' [\mathbf{A}_\sigma^{-1}(t)]_{ij} [\langle V_{j\sigma}^{\rm SI}(t)\rangle - \langle w_{j\sigma}(t)\rangle], \tag{13}$$

where

$$[\mathbf{A}_\sigma(t)]_{ij} = \delta_{ij} - \iiint \frac{n_{i\sigma}(\mathbf{r},t) n_{j\sigma}(\mathbf{r},t)}{n_\sigma(\mathbf{r},t)} d^3\mathbf{r}, \tag{14}$$

and

$$\langle V_{j\sigma}^{\rm SI}(t)\rangle = \iiint V_\sigma^{\rm SI}(\mathbf{r},t) n_{j\sigma}(\mathbf{r},t) d^3\mathbf{r}. \tag{15}$$

The LDA-SIC is an exchange-only approximation, so that electrons with opposite spins do not interact. For noble-gas atoms in particular, the number of linearly independent KS

equations to be solved is therefore $Z/2$. The total density can then be found by multiplying the spin-up (or -down) electron density by 2.

B. Interaction potential

The time-dependent interaction potential due to a dressing IR laser field of frequency ω_o and an APT of central frequency $\bar{N}\omega_o$, both polarized along the z-axis, is

$$\mathbf{r}\cdot\mathbf{E}(t) = \left[E_{\rm IR}(t)\sin(\omega_o t) + E_{\rm xuv}(t')\cos\left(\bar{N}\omega_o t'\right)\right] r\cos\theta, \tag{16}$$

where $t' \equiv t - \alpha/\omega_o$ is the time delay, with α being a phase delay, between the IR field and the APT, and $E_{\rm IR}(t)$ is a pulse envelope function of the IR field, given by

$$E_{\rm IR}(t) = \sqrt{I_o}\cos^2\left(\frac{\omega_o t}{2n}\right), \tag{17}$$

with I_o and n being the peak intensity and the number of optical cycles ($T = 2\pi/\omega_o$) per pulse, respectively. The function $E_{\rm xuv}(t)$ is a train of narrow ($\sim$ 300 fs) $\cos^2$ functions, separated by either $T/2$ or T. In Figure 1, we plot an example of such fields near the peak of the IR pulse ($t = 0$) for $\alpha = 0$. Fig. 1(a) is the case where the separation of XUV pulses is a half-optical cycle and happens when the XUV pulses are synthesized from odd high harmonics generated with a monochromatic IR field of frequency ω_o. On the other hand, XUV pulses in Fig. 1(b) are separated by a full-optical cycle of the IR field, which happens when they are synthesized from both even and odd high harmonics generated with a two-color IR field of fundamental frequency ω_o and its second harmonic $2\omega_o$ [26]. For a time-resolved measurement of photoelectron momentum distributions, the type of fields in Fig. 1(b) must be used, to record at the same phase of an IR field for all XUV pulses, and the phase delay α is varied between 0 and 2π for a stroboscopic measurement [16]. On the other hand, the type of fields in Fig. 1(a) is useful in eliminating interferences between resonant two- or three-photon transition and non-resonant one-photon transitions in the PMDs, as we demonstrate in Sec. III.

Because of the azimuthal symmetry in (16), the magnetic quantum number m_i of the i-th orbital is conserved during the time evolution, so that we can assume the solution of form

$$\psi_{i\sigma}(\mathbf{r},t) = \sum_{\ell} \frac{R_{i\sigma}^{\ell(m_i)}(r,t)}{r} Y_\ell^{(m_i)}(\theta,\phi). \tag{18}$$

It then follows that the spin electron density of each orbital (3) is independent of azimuthal angle ϕ. The details of numerical calculation based on the generalized pseudospectral method [27] is given in Ref. [20].

C. Photoelectron momentum distribution

In each timestep, the wavefunction $\psi_{i\sigma}(\mathbf{r},t)$ is split into inner and outer regions by a smooth masking function $f(r)$, and the PMD is found from the outer-region wavefunction that is propagated in the momentum space with the Volkov Hamiltonian in the velocity gauge [28]. That is,

$$\psi_{i\sigma}(\mathbf{r},t) = f(r)\psi_{i\sigma}(\mathbf{r},t) + [1-f(r)]\psi_{i\sigma}(\mathbf{r},t) = \psi_{i\sigma}^{(\mathrm{in})}(\mathbf{r},t) + \psi_{i\sigma}^{(\mathrm{out})}(\mathbf{r},t), \tag{19}$$

The function $f(r)$ is one in the inner region ($0 \le r \le R_b$) and smoothly decreases to zero in the outer region ($R_b < r < r_{\max}$). In our calculations, R_b is set at five times the classical oscillator radius ($= \sqrt{I_o}/{\omega_o}^2$) or 20 a.u., whichever is larger, whereas $r_{\max}$ is set at 100 a.u. It has been tested that using larger R_b or $r_{\max}$ does not affect the resulting PMD.

We study the PMD of individual atomic orbital given by

$$D_{i\sigma}(p,\theta_p) = \left|\tilde{\psi}_{i\sigma}^{\mathrm{v}}(\mathbf{p},t_\infty)\right|^2, \tag{20}$$

where $\tilde{\psi}_{i\sigma}^{\mathrm{v}}(\mathbf{p},t_\infty)$ is the Fourier transform of the outer-region wavefunction at the end of the time evolution $t = t_\infty$, as well as the total PMD of all atomic orbitals given by

$$D(p,\theta_p) = \left|\sum_{\sigma}\sum_{i=1}^{N_\sigma} \tilde{\psi}_{i\sigma}^{\mathrm{v}}(\mathbf{p},t_\infty)\right|^2. \tag{21}$$

III. RESULTS

A. Helium

1. *Resonant two-photon ionization of He*

Figure 2 shows a level diagram for R2PI and R3PI of a He atom using an IR laser field and its 15th harmonic (15H), in accordance with the experiment by Villeneuve *et al.* [21]. Field-free energies of Kohn-Sham wavefunctions in bound- and excited-states are given on

the right-hand side of the diagram. Because of the broadband high harmonics used to produce an APT, XUV excitation in a time-resolved PMD measurement is not restricted to the 15H energy only but also to the energies of its neighbouring harmonics as well. As a result, the time-resolved PMD of an atom dressed by an IR laser field and probed by an APT produced from its high harmonics has multiple concentric peaks at the radii given by

$$|p| = \sqrt{2(s\,\omega_o + N\,\omega_o - I_p - U_p)}, \tag{22}$$

where $s = \pm 1, \pm 2, \ldots$ is the number of IR photons absorbed (+) or emitted (-), $N\omega_o$ is an XUV photon energy contained in the APT, I_p is the ionization potential, and $U_p = I_o(4\,{\omega_o}^2)^{-1}$ is the ponderomotive energy of a dressing IR field. The single ionization potential of an atom in the density functional theory is equal to the negative of the ground-state energy of the highest occupied Kohn-Sham orbital [22], and therefore $I_p = 24.98$ eV for a He atom in our calculations.

In Fig. 2, the two lowest momenta $|p|$ of an ionized electron given by Eq. (22) following non-resonant, one-photon absorption ($N = 16$ or 17, and $s = 0$) in the absence of an IR field ($U_p = 0$) are shown in atomic units. When a dressing IR field is turned on, the momentum $|p|$ for absorption of a 16H-photon is also reachable through R2PI (15H + ω_o or 17H - ω_o) as well. To elaborate this point, we plot the PMDs of a He atom driven by an APT alone (i.e., without a dressing IR field) of central energy $\bar{N}\omega_o = 23.54$ eV (corresponding to the 15H of the 790-nm field) in Figures 3(a) and (b) when XUV pulses in the APT are separated by a half-optical cycle and a full-optical cycle, respectively. Notice that the PMDs in both cases have multiple concentric peaks, despite the fact that there are no IR photons to produce sidebands in these calculations. This is in contrast to the measurement using a monochromatic XUV pulse of longer duration ($\gg 1$ fs) as in Ref. [18], which yields a single peak in the PMD in the absence of a dressing IR field. Even-ordered peaks (16H, 18H, ...) are missing in Fig. 3(a) because they are measured with an APT containing only odd-ordered high harmonics produced with a monochromatic IR field; see discussions of Fig. 1(a) in the previous section. On the other hand, if the driving laser field of HHG is two-colored, containing the fundamental frequency ω_o and its second harmonic $2\omega_o$, then both even and odd harmonics are contained in an APT, so that the PMD has multiple peaks separated by the fundamental frequency ω_o, as shown in Fig. 3(b). The location of peaks in Figs. 3(a) and (b) agrees with the momentum values given by Eq. (22) with $s = 0$, $N = 16, 17, ...,$

and $U_p = 0$ (no IR field). The electron density distribution at $|p| = 0.1$ in Fig. 3(b) has the dipole-like odd symmetry of a P-wave, indicating a nonresonant transition from the 1s ground state via absorption of a 16H photon. It has a purely odd symmetry, as there is no sidebands caused by an IR photon in Figs. 3(a) and (b).

When an dressing IR field is added to an APT in a time-resolved PMD measurement, sidebands are produced around XUV peaks separated by $\pm\omega_o$ [11]. In addition, the ionization threshold would be up-shifted by a ponderomotive energy U_p [29]. In Fig. 3(c), we plot the PMD of a He atom driven by a 20-cycle, IR (790 nm) laser pulse of peak intensity $I_o = 1\times10^{11}$ W/cm^2 and an APT of XUV pulses (23.54 eV) that are separated by 1a half-optical cycle of the dressing field with no phase delay, as shown in Fig. 1(a). The ponderomotive energy U_p at such a weak intensity is negligibly small (~ 0.006 eV). In contrast to the XUV-only calculation in Fig. 3(a), there is a high concentration of electron distribution in Fig. 3(c) at $|p| = 0.1$, corresponding to the energy of an ionized electron via R2PI (15H + ω_o). The distribution has a 4-lobe, even symmetry of a D-wave, as predicted in Fig. 2. The narrow distribution at $|p| = 3.5$ corresponds to the single-photon ionization by the 17th harmonic. The APT used to generate the PMD in Fig. 3(c) does not contain 16H photons, and therefore its electron density at $|p| = 0.1$ is assured to have a purely even symmetry.

The separation of XUV pulses in an APT used to produce Fig. 3(c) is a half-optical cycle. By changing it to a full-optical cycle and introducing a phase delay α with respect to the dressing IR laser field, we can coherently probe the electron dynamics during R2PI. This is demonstrated in Figure 4, where we plot the time-resolved PMDs generated by such a field as shown in Fig. 1(b), for three different phase delays α. All the laser parameters remain the same as in Fig. 3(c) except for the separation of XUV pulses in an APT. We find in Fig. 4 that the electron distributions at $|p| = 0.1$ no longer show the 4-lobe structure that was present in Fig. 3(c). It is likely that interferences between the resonant transition from the $1s3p\,^1P$ excited state (15H + ω_o) and the non-resonant transition via absorption of a 16H photon, which coexist with the type of an APT shown in Fig. 1(b), destroyed the clear display of even/odd symmetry in the PMDs of Fig. 4 at $|p| = 0.1$. For phase delays $\alpha = 0$ and π, when XUV pulse in an APT coincides with the zero-crossing of the IR field, the PMD is shifted in the direction of laser polarization axis, reflecting the periodic motion an ionized electron driven by an IR laser field in the configuration space [16].

2. Resonant three-photon ionization of He

Figure 5 shows the time-resolved PMDs following resonant three-photon ionization (R3PI) of a He atom induced by a 20-cycle, 820-nm laser pulse of various peak intensities ($10^{11} - 10^{13}$ W/cm^2) and an APT ($\bar{N}\omega_o = 22.68$ eV) whose XUV pulses are separated by a half-optical cycle and synchronized at each zero-crossing of the dressing IR field, as shown in Fig. 1(a). The R3PI transition we study is schematically depicted in Fig. 2; the ground-state electron is resonantly excited first to the $1s2p\,^1P$ state via absorption of 15H photon, next to the $1s3d\,^1D$ excited state via absorption of an IR photon, before ionizing to free partial waves by absorption of another IR photon. The PMD of an ionized electron via R3PI is then expected to have an odd (P, F, ...) symmetry, as indicated in Fig. 2. Alternatively, an electron can ionize non-resonantly via absorption of a 17H photon in Fig. 5, which should also produce a partial wave of odd symmetry.

When driven by the lowest-intensity IR fields ($I_o = 1 \times 10^{11}$ W/cm^2), the electron distribution in Fig. 5 is dipole-like and narrowly concentrated along a concentric circle of radius $|p| = 0.23$, which corresponds to the single-photon ionization by 17th harmonic contained in an APT. It has odd symmetry of a P-wave, as expected. As the peak intensity of a dressing IR pulse increases to $I_o = 2 \times 10^{12}$ W/cm^2 in Fig. 5, the amount of electron density at $|p| = 0.23$ becomes 4 times higher, and another narrow, concentric peak appears at a radius $|p| = 0.40$, corresponding to the energy of 18H. The one-photon excitation via 18th harmonic is not possible when XUV pulses in the APT are separated by a half-optical cycle. It must therefore be interpreted as a sideband (17H + ω_o) produced by an IR photon. For higher intensities above $I_o = 4 \times 10^{12}$ W/cm^2, the PMDs at $|p| = 0.23$ exhibit a 6-lobe, odd symmetry of an F-wave, as expected in R3PI of Fig. 2. The radius of these 6-lobe distributions decreases as the driving-laser intensity increases, in agreement with the finding in Villeneuve *et al.* [21], because of the up-shift of an ionization threshold by the ponderomotive energy U_p of a dressing IR field.

In Figure 6, we plot the time-resolved PMD driven by a 20-cycle, 820-nm laser pulse of peak intensity $I_o = 1 \times 10^{13}$ W/cm^2 and probed by an APT (22.68 eV) whose XVU peaks are separated by a full-optical cycle, for three different phase delays α. With such an APT, non-resonant transition by a 17H or a 18H photon is possible as well as R3PI. As a result, the PMD in Fig. 6 at the lowest peak ($|p| = 0.23$) may contain ionized electron density

from three different transitions: R3PI (15H + ω_o + ω_o), a single-photon absorption (17H), and a single-photon absorption followed with an IR photon emission (18H - ω_o), for which the ionized partial waves should have odd, odd, and even symmetry, respectively. Similarly to the R2PI cases in Fig. 4, the PMDs captured by the APT whose pulse separation is a full-optical cycle in Fig. 6 do not show a clear even/odd symmetry except when the phase delay is $\alpha = \pi/2$, due to interference of three different transitions induced by an APT in this case.

B. Neon

Figure 7 shows a level diagram for R2PI of a Ne atom. We use a 785-nm dressing laser and its 13th harmonic (20.54 eV) to induce the process in our calculation. The IR laser pulse used in Villeneuve *et al.* [21] had a slightly longer wavelength (800 nm), but the energy of its 13th harmonic (20.15 eV) is not quite large enough for a resonant transition between the $2p$ ground state and the $3d$ excited state of an valence electron theoretically. Field-free energies of Kohn-Sham wavefunctions in the ground- and excited-state levels in eV are given on the right-hand side of the diagram. The single ionization potential of a Ne atom according to the density functional theory is $I_p = 21.98$ eV. Also shown in Fig. 7 are the two lowest momenta $|p|$ of non-resonant one-photon absorption of a 14H or a 15H photon above ionization threshold given by Eq. (22) in the absence of an IR laser field ($U_p = 0$).

In Figure 8, we plot the time-resolved PMDs of all electrons in a Ne atom given by Eq. (21), during the R2PI driven by a 20-cycle, 785-nm laser pulse of various peak intensities and an APT ($\bar{N}\omega_o = 20.54$ eV) whose XUV pulses are separated by a half-optical cycle. For a comparison, the Ne-atom PMDs measured with an IR (800 nm) driving laser field of the three lowest peak intensities in Fig. 8 ($I_o = 5\times10^{11}$, 2×10^{12}, and 4×10^{12} W/cm^2) are given in the supplementary material of Villeneuve *et al.* [21]. The amount of electron density in the PMD in Fig. 8 is largest when $I_o = 2\times10^{12}$ W/cm^2, in accordance to their measurement. Villeneuve *et al.* reported the 6-lobe, even symmetry of an F-wave in the PMD of a Ne atom, and we find a similar structure in our calculation at $I_o = 1\times10^{13}$ W/cm^2 in Fig. 8.

One striking difference between the PMDs of a Ne atom in Fig. 8 and of a He atom in Fig. 5 is that the symmetry with respect to the p_x-axis is lost in the former but not in the latter. This is caused by the interference among valence electrons ionized from the

degenerate $2p$-orbital of a Ne atom. To illustrate such an effect of orbital interference, we plot in Figure 9 the PMDs of individual orbitals given by Eq. (20) of a Ne atom at $I_o = 8 \times 10^{12}$ W/cm^2. The electron density in the PMD of a $1s$-electron turned out to be in the order of 10^{-16}, more than 8 orders of magnitude smaller than the rest of the electrons in a Ne atom, and therefore its PMD is not shown. The symmetry with respect to the p_x-axis is preserved in Fig. 9, which shows that the symmetry breaking of the all-electron PMD in Fig. 8 is a result of orbital-orbital interference. The contribution from the $2s$ orbital in Fig. 9 is several orders of magnitude smaller than the $2p$ valence orbitals', and therefore we can disregard its influence to the total PMD in Fig. 8. (It is nevertheless worthwhile to mention the symmetry in the PMD of the $2s$ orbital in Fig. 9; it has an odd symmetry of an F-wave, which implies that the 2s orbital underwent some kind of resonant few-photon ionization not described in Fig. 7, presumably R3PI through the $4d$ excited state by absorption of two 15H photons followed by absorption of one IR photon.) The amount of electron density from the $2p$ orbital is largest in the $m = 0$ channel, but contributions from two electrons in the $m = \pm 1$ states are sufficiently strong to affect the total PMD and break its symmetry in Fig. 8. We also notice in Figs. 9(b) and (c) that there is a clearly distinguishable trace of both P and F partial waves appearing in these $2p$-orbital PMDs (i.e., the 6-lobe and 2-lobe electron distributions at radii of $|p| = 0.5$ and $|p| = 0.1$, respectively), although it was only the F-wave observed in Villeneuve *et al.* [21]. Such a simultaneous appearance of two partial waves should be possible in resonant two-color few-photon transitions, as long as they are of the same parity.

Finally, in Figure 10, we plot the time-resolved PMDs of a Ne atom driven by a 20-cycle, 785-nm IR laser pulse of peak intensity $I_o = 1 \times 10^{13}$ W/cm^2 and probed by an APT of XUV pulses (20.54 eV) separated by a full-optical cycle, for three different phase delays. The PMD at $|p| = 0.1$ may contain ionized electron density from three different transitions: R2PI (13H + ω_o), a single-photon absorption (14H), and a single-photon absorption followed with an IR photon emission (15H - ω_o), for which the ionized partial waves should have odd, even, and odd symmetry, respectively. In addition to the interference among these three different transitions, valence electrons from the degenerate $2p$-orbital should also interfere and introduce symmetry breaking between the positive and negative directions of a laser polarization, as we have seen in Fig. 8. It is therefore not possible to attribute only the F-wave to the time-resolved PMD of a Ne atom and describe its time evolution during 2PRI,

although such a model was provided in Villeneuve *et al.* [21]. The PMDs we obtained from the all-electron calculation based on the time-dependent Kohn-Sham equations in Fig. 10 show very complex interferences which must come from multiple transitions and a degenerate orbital.

IV. CONCLUSION

In this paper, we presented an all-electron, ab initio calculation of time-resolved photoelectron momentum distribution (PMD) of He and Ne atoms during resonant two- or three-photon ionization, based on the numerical solution of the time-dependent Kohn-Sham equations. Our calculation shows that one can resonantly ionize an excited-state electron by a broadband, attosecond pulse train (APT) if its extreme ultraviolet (XUV) pulses are separated by a half-optical cycle of a infrared (IR) dressing laser field. The selection of a particular excited state is achieved by adjusting the frequency and intensity of the IR laser pulse, and it can be verified by observation of symmetry in the PMD. The stroboscopic observation of PMD during the resonant two- or three-photon ionization is also possible by adding a second harmonic to the driving IR laser field which changes a separation of XUV pulses in an APT to a full-optical cycle. The stroboscopic measurement of a PMD, however, is prone to introduce interferences between the resonant and non-resonant transitions, as exemplified by a broken symmetry in the PMD. The PMD of a Ne atom is subject to an additional kind of interferences between electrons ionizing from the degenerate $2p$-orbital even when the effect of non-resonant one-photon transition is eliminated by using an APT synchronized at each zero-crossing of a dressing IR field at half-optical cycle.

ACKNOWLEDGMENTS

This work was supported by the U.S. Department of Energy under Contract No. DE-FG02-06ER46304. Numerical calculation was done on Indiana State University's quantum cluster and high-performance computer (silicon). The research used resources of the National Energy Research Scientific Computing Center, which is supported by the Office of Science

of the U.S. Department of Energy under Contract No. DE-AC02-05CH11231.

---

[1] V. Schmidt, N. Sandner, H. Kuntzemüller, P. Dhez, F. Wuilleumier, and E. Källne, Phys. Rev. A **13**, 1748 (1976).

[2] B. Walker, B. Sheehy, L. F. DiMauro, P. Agostini, K. J. Schafer, and K. C. Kulander, Phys. Rev. Lett. **73**, 1227 (1994).

[3] R. ling Chien, O. C. Mullins, and R. S. Berry, Phys. Rev. A **28**, 2078 (1983).

[4] R. Moshammer, Y. H. Jiang, L. Foucar, A. Rudenko, T. Ergler, C. D. Schröter, S. Lüdemann, K. Zrost, D. Fischer, J. Titze, T. Jahnke, M. Schöffler, T. Weber, R. Dörner, T. J. M. Zouros, A. Dorn, T. Ferger, K. U. Kühnel, S. Düsterer, R. Treusch, P. Radcliffe, E. Plönjes, and J. Ullrich, Phys. Rev. Lett. **98**, 203001 (2007).

[5] P. Lambropoulos, L. A. A. Nikolopoulos, and M. G. Makris, Phys. Rev. A **72**, 013410 (2005).

[6] A. A. Sorokin, M. Wellhöfer, S. V. Bobashev, K. Tiedtke, and M. Richter, Phys. Rev. A **75**, 051402 (2007).

[7] A. Rudenko, L. Foucar, M. Kurka, T. Ergler, K. U. Kühnel, Y. H. Jiang, A. Voitkiv, B. Najjari, A. Kheifets, S. Lüdemann, T. Havermeier, M. Smolarski, S. Schössler, K. Cole, M. Schöffler, R. Dörner, S. Düsterer, W. Li, B. Keitel, R. Treusch, M. Gensch, C. D. Schröter, R. Moshammer, and J. Ullrich, Phys. Rev. Lett. **101**, 073003 (2008).

[8] A. Rudenko, Y. H. Jiang, M. Kurka, K. U. Kuhnel, L. Foucar, O. Herrwerth, M. Lezius, M. F. Kling, C. D. Schroter, R. Moshammer, and J. Ullrich, J. Phys. B: At. Mol. Opt. Phys. **43**, 203004 (2010).

[9] R. Ma, K. Motomura, K. L. Ishikawa, S. Mondal, H. Fukuzawa, A. Yamada, K. Ueda, K. Nagaya, S. Yase, Y. Mizoguchi, M. Yao, A. Rouze, A. Hundermark, M. J. J. Vrakking, P. Johnsson, M. Nagasono, K. Tono, T. Togashi, Y. Senba, H. Ohashi, M. Yabashi, and T. Ishikawa, J. Phys. B: At. Mol. Opt. Phys. **46** (2013).

[10] K. L. Ishikawa and K. Ueda, Phys. Rev. Lett. **108**, 033003 (2012).

[11] M. Meyer, D. Cubaynes, P. O'Keeffe, H. Luna, P. Yeates, E. T. Kennedy, J. T. Costello, P. Orr, R. Taïeb, A. Maquet, S. Düsterer, P. Radcliffe, H. Redlin, A. Azima, E. Plönjes, and J. Feldhaus, Phys. Rev. A **74**, 011401 (2006).

[12] M. Meyer, P. Radcliffe, T. Tschentscher, J. T. Costello, A. L. Cavalieri, I. Grguras, A. R. Maier, R. Kienberger, J. Bozek, C. Bostedt, S. Schorb, R. Coffee, M. Messerschmidt, C. Roedig, E. Sistrunk, L. F. DiMauro, G. Doumy, K. Ueda, S. Wada, S. Dusterer, A. K. Kazansky, and N. M. Kabachnik, Phys. Rev. Lett. **108**, 063007 (2012).

[13] S. Dusterer, L. Rading, P. Johnsson, A. Rouzée, A. Hundertmark, M. J. J. Vrakking, P. Radcliffe, M. Meyer, A. K. Kazansky, and N. M. Kabachnik, Journal of Physics B: Atomic, Molecular and Optical Physics **46**, 164026 (2013).

[14] B. Manschwetus, L. Rading, F. Campi, S. Maclot, H. Coudert-Alteirac, J. Lahl, H. Wikmark, P. Rudawski, C. M. Heyl, B. Farkas, T. Mohamed, A. L'Huillier, and P. Johnsson, Phys. Rev. A **93**, 061402 (2016).

[15] J. Mauritsson, P. Johnsson, E. Mansten, M. Swoboda, R. Ruchon, A. L'Huillier, and K. J. Schafer, Phys. Rev. Lett. **100**, 073003 (2008).

[16] J. Mauritsson, M. B. Gaarde, and K. J. Schafer, Phys. Rev. A **72**, 013401 (2005).

[17] M. Swoboda, T. Fordell, K. Klunder, J. M. Dahlstrom, M. Miranda, C. Buth, K. J. Schafer, J. Mauritsson, A. L'Huillier, and M. Gisselbrecht, Phys. Rev. Lett. **104**, 103003 (2010).

[18] L. H. Haber, B. Doughty, and S. R. Leone, Phys. Rev. A **84**, 013416 (2011).

[19] A. Fleischer, H. J. Wörner, L. Arissian, L. R. Liu, M. Meckel, A. Rippert, R. Dörner, D. M. Villeneuve, P. B. Corkum, and A. Staudte, Phys. Rev. Lett. **107**, 113003 (2011).

[20] M. Murakami, G. P. Zhang, and S.-I. Chu, Phys. Rev. A **95**, 053419 (2017).

[21] D. M. Villeneuve, P. Hockett, M. J. J. Vrakking, and H. Niikura, Science **356**, 1150 (2017).

[22] J. P. Perdew and A. Zunger, Phys. Rev. B **23**, 5048 (1981).

[23] X.-M. Tong and S.-I. Chu, Phys. Rev. A **55**, 3406 (1997).

[24] J. B. Krieger, Y. Li, and G. J. Iafrate, Phys. Rev. A **46**, 5453 (1992).

[25] C. A. Ullrich, U. J. Gossmann, and E. K. U. Gross, Phys. Rev. Lett. **74**, 872 (1995).

[26] J. Mauritsson, P. Johnsson, E. Gustafsson, A. L'Huillier, K. J. Schafer, and M. B. Gaarde, Phys. Rev. Lett. **97**, 013001 (2006).

[27] X.-M. Tong and S.-I. Chu, Chemical Physics **217**, 119 (1997).

[28] X. M. Tong, K. Hino, and N. Toshima, Phys. Rev. A **74**, 031405(R) (2006).

[29] M. Murakami and S.-I. Chu, Phys. Rev. A **88**, 043428 (2013).

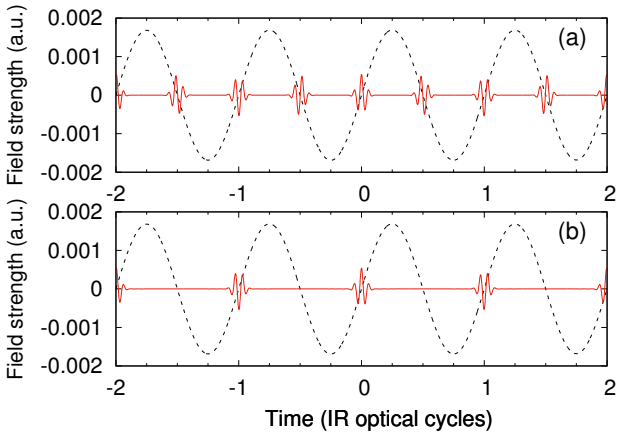

FIG. 1. (Color online) Driving laser fields used for the resonant two-photon ionization. Infrared (IR) fields are drawn with dashed lines, whereas attosecond pulse trains (APTs) are drawn with solid lines. In these plots, the peak intensity of the IR field is $I_o = 1 \times 10^{11}$ W/cm^2, but it is increased up to 10^{13} W/cm^2 in our calculations in Sec. III. The intensity and full-width-half-maximum duration of each extreme-ultraviolet (XUV) pulse in an APT, on the other hand, are fixed at 10^{10} W/cm^2 and ~ 300 as in all calculations, as shown in these plots. The phase delay between an IR field and an APT is zero in these examples.

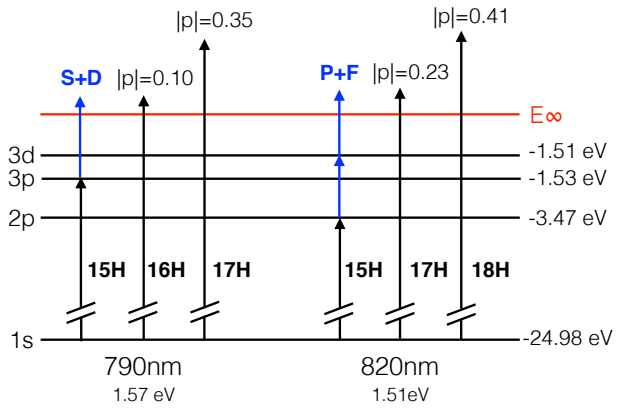

FIG. 2. (Color online) (a) Level diagram for the resonant two- or three-photon ionization of a He atom driven by a 790-nm or an 820-nm laser field, as well as an XUV pulse-train of central energy at the 15th harmonic (15H), which is 23.54 eV or 22.68 eV, respectively. Field-free energy of each Kohn-Sham orbital obtained with the density functional theory is given on the right-hand side. Because of the selection rule in dipole transitions, an ionized electron in each case is expected to have even (S, D,...) or odd (P, F,...) symmetry, as indicated in the figure. Also shown are the two lowest momenta $|p|$ (in atomic units) of an ionized electron following the one-photon (16-18H) absorption. Note that an even-order high harmonics such as 16H and 18H are contained in an APT only if the driving laser for HHG is two-colored, consisting of an IR field and its second harmonic, so that the separation of each XUV pulses becomes a full-optical cycle as shown in Fig. 1(b). At the peak of a driving-laser field, the ionization threshold (E_∞) is up-shifted by an amount of ponderomotive energy of the field which is roughly $0.006 \sim 0.6$ eV when the peak intensity is $I_o = 10^{11} \sim 10^{13}$ W/cm^2.

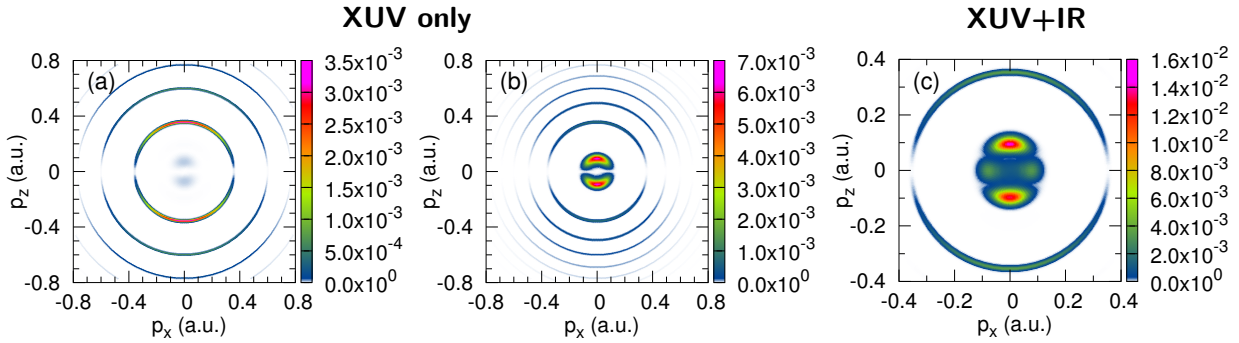

FIG. 3. (Color online) Photoelectron momentum distributions (PMDs) of a He atom driven by a train of XUV pulses of central energy 23.54 eV (corresponding to the 15th harmonic of the 790-nm IR field) that are either separated by (a) a half-optical cycle of the IR field, or (b) a full-optical cycle of the IR field. (c) The PMD of a He atom driven by an IR (790 nm), 20-cycle laser pulse of peak intensity $I_o = 1 \times 10^{11}$ W/cm^2, as well as a train of XUV (23.54 eV) pulses that are separated by a half-optical optical cycle of the IR field. The phase delay between the IR field and the XUV pulses is fixed at $\alpha = 0$, so that each XUV pulse coincides with the zero-crossing of the IR field, as shown in Fig. 1(a).

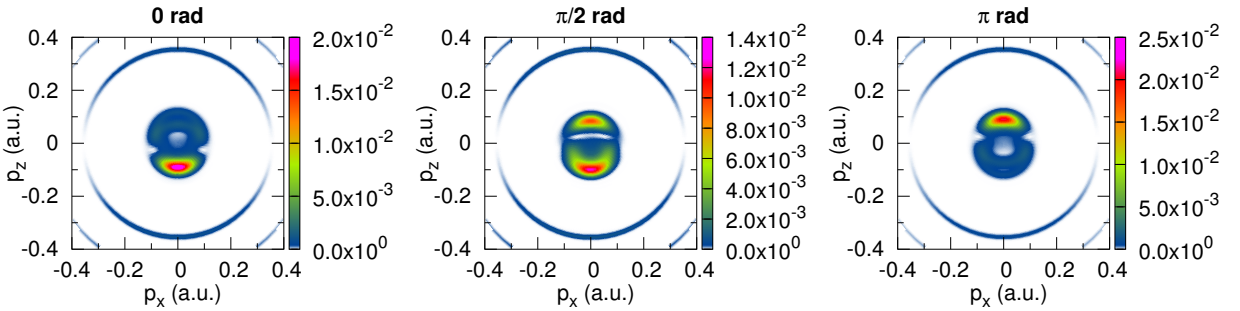

FIG. 4. (Color online) The same as Fig. 3(c), but the separation of XUV pulses are changed to a full optical cycle as shown in Fig. 1(b) for stroboscopic measurements. The phase delays α of XUV pulses with respect to the IR field of frequency ω_o, which allows a stroboscopic measurement at $t' \equiv t - \alpha/\omega_o$ within a subcycle time frame, are indicated at the top of each plots.

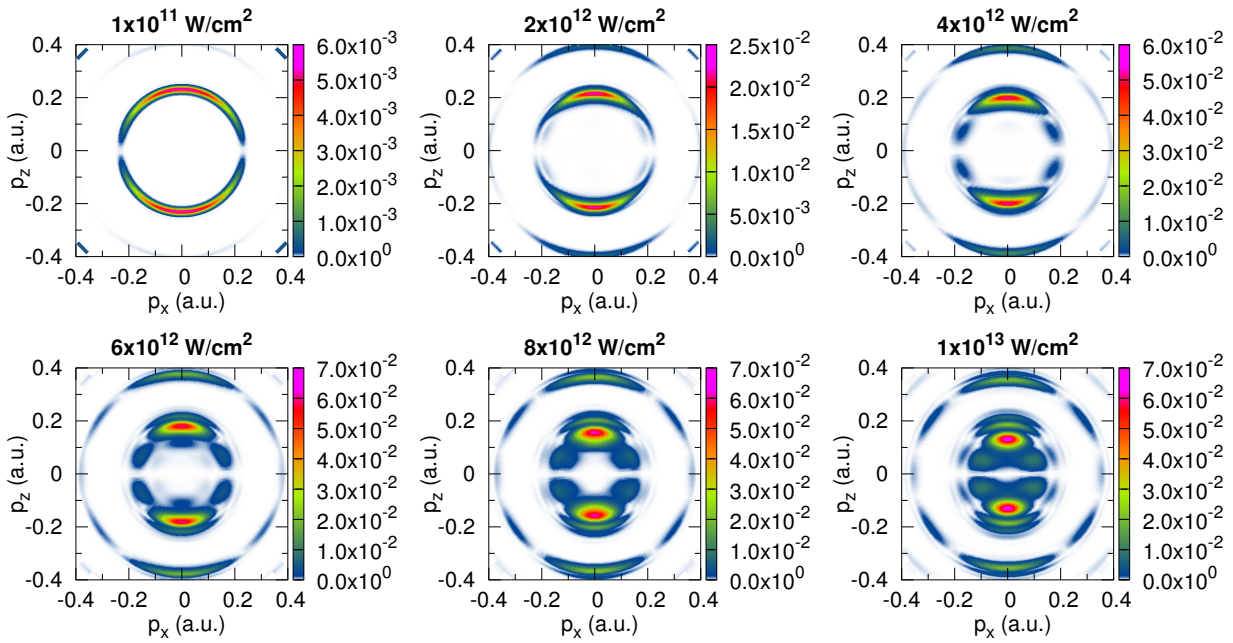

FIG. 5. (Color online) PMDs of a He atom driven by an IR field of wavelength 820 nm and various peak intensities, as shown at the top of each plot, and a train of XUV pulses of energy 22.68 eV (corresponding to the 15th harmonic of the IR field) that are separated by 1/2 of the IR optical cycle and synchronized at each zero-crossing of the IR field, as shown in Fig. 1(a).

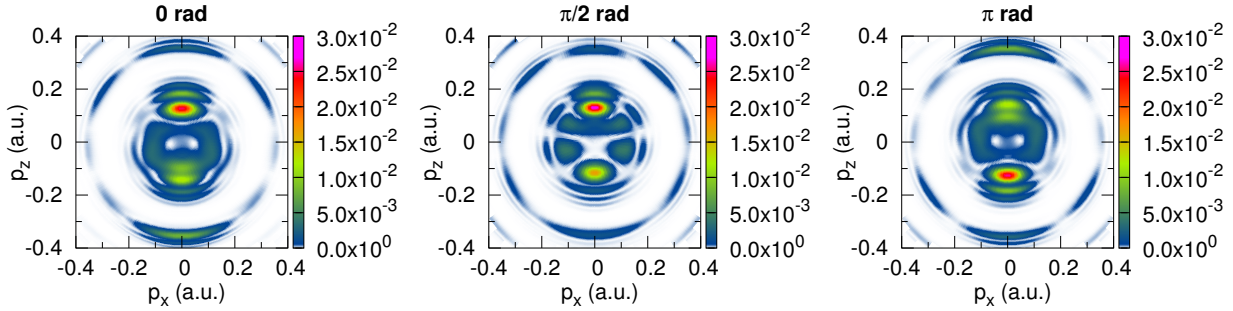

FIG. 6. (Color online) Stroboscopic measurements of PMDs of a He atom using an 820-nm IR field and 22.68-eV pulse trains that are separated by a full optical cycle as shown in Fig. 1(b), at time $t' \equiv t - \alpha/\omega_o$ where ω_o is the IR frequency and α is a phase delay indicated at the top of each plot. The peak intensity of the IR field is $I_o = 1 \times 10^{13}$ W/cm^2.

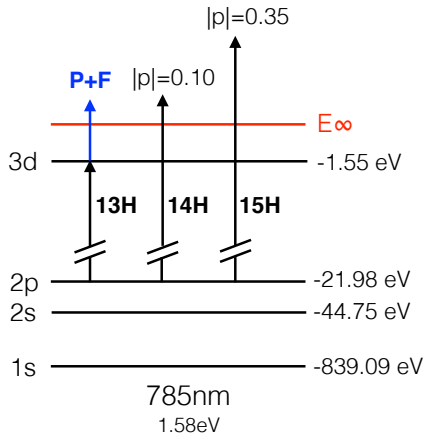

FIG. 7. (Color online) Level diagram for the resonant two-photon ionization of a Ne atom driven by an IR (785 nm) laser field and an XUV attosecond pulse train (APT) of central energy 20.54 eV, corresponding to the 13th harmonic (13H) of the IR field. For simplicity, only the transitions for valence electrons in the 2p shell are considered. Field-free energy of each Kohn-Sham orbital obtained with the density functional theory is given on the right-hand side. An ionized electron in each case is expected to have odd (P, F,...) symmetry, as indicated in the figure. Also shown in each case are the two lowest momenta $|p|$ of an ionized electron following one-photon (14,15H) absorption in atomic units. Note that an even-order high harmonics such as 14H are contained in an APT only if the driving laser for HHG is two-colored, consisting of an IR field and its second harmonic, so that the separation of each XUV pulses is a full-optical cycle as shown in Fig. 1(b).

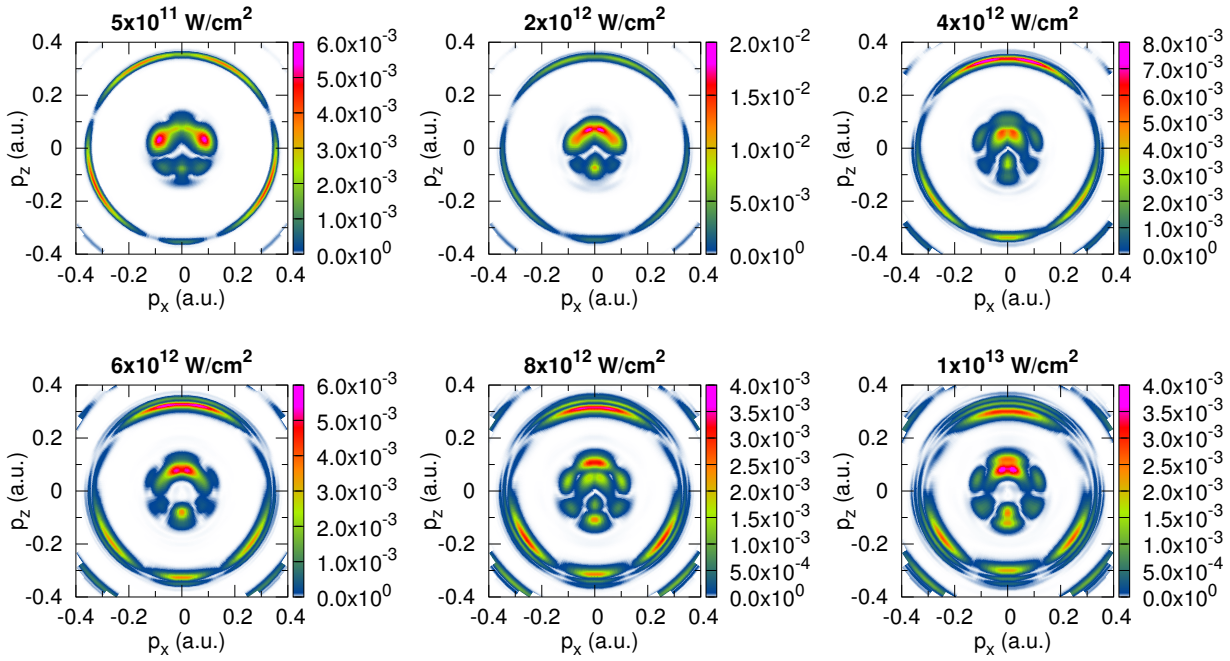

FIG. 8. (Color online) PMDs of a Ne atom driven by an IR field of wavelength 785 nm and various peak intensities, as shown at the top of each plot, and a train of XUV pulses of energy 20.54 eV (corresponding to the 13th harmonic of the IR field) that are separated by 1/2 of the IR optical cycle and synchronized at each zero-crossing of the IR field, as shown in Fig. 1(a).

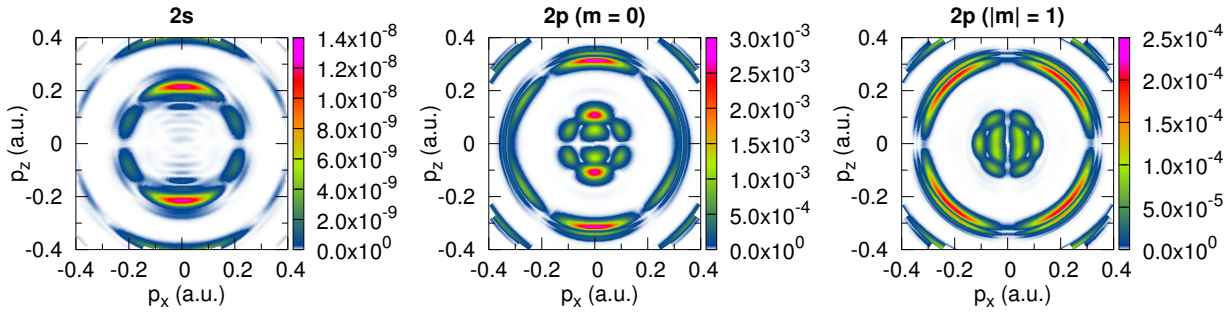

FIG. 9. (Color online) For the total PMD of a Ne atom in Fig. 8 driven at the peak driving-laser intensity of $I_o = 8 \times 10^{12}$ W/cm^2, the corresponding PMDs of individual Kohn-Sham orbitals given by Eq. (20) are shown. Labels on the top of each plot denote the initial state of an orbital.

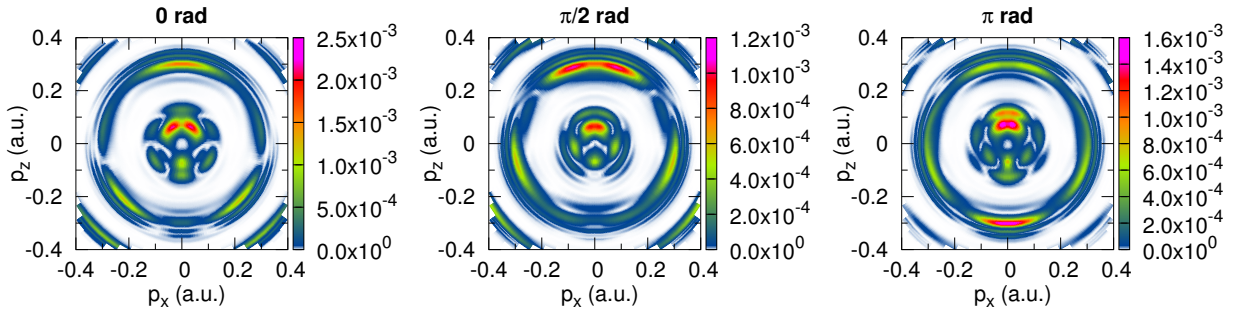

FIG. 10. (Color online) Stroboscopic measurements of PMDs of a Ne atom using a 20-cycle, IR (785 nm) laser field and an APT of XUV pulses of central energy 20.54 eV that are separated by a full optical cycle of the IR field, as shown in Fig. 1(b), at time $t' \equiv t - \alpha/\omega_o$ where ω_o is the IR frequency and α is a phase delay indicated at the top of each plot. The peak intensity of the IR field is $I_o = 1 \times 10^{13}$ W/cm^2.